Received: 15 June 2024 | Revised: 29 October 2024 | Accepted: 24 March 2025

DOI: 10.1002/aic.18844

AIChE JOURNAL

RESEARCH ARTICLE

Thermodynamics and Molecular-Scale Phenomena

Microscopic kinetics of scission and reformation in the pyrolysis of nitrocellulose

Changwei Liu[1] | Haojie Qian[1] | Qing Wang[2] | Jinkai Qiu[1,2] | Yajun Ding[3] | Cheng Lian[1,2] | Honglai Liu[1,2]

[1]State Key Laboratory of Chemical Engineering, School of Chemical Engineering, East China University of Science and Technology, Shanghai, People's Republic of China

[2]School of Chemistry and Molecular Engineering, East China University of Science and Technology, Shanghai, People's Republic of China

[3]School of Chemistry and Chemical Engineering, Nanjing University of Science and Technology, Nanjing, People's Republic of China

Correspondence
Yajun Ding, School of Chemistry and Chemical Engineering, Nanjing University of Science and Technology, Nanjing 210094, People's Republic of China.
Email: dyj@njust.edu.cn

Cheng Lian, State Key Laboratory of Chemical Engineering, School of Chemical Engineering, East China University of Science and Technology, Shanghai 200237, People's Republic of China.
Email: liancheng@ecust.edu.cn

Funding information
National Key Research and Development Program of China, Grant/Award Number: 2019YFC1906702; Fundamental Research Funds for the Central Universities, Grant/Award Numbers: 2022ZFJH004, 2024SMECP05; National Natural Science Foundation of China, Grant/Award Number: 22475101; Young Elite Scientists Sponsorship Program by CAST, Grant/Award Number: 2022QNRC001

Abstract

Nitrocellulose (NC) is essential in high-energy propellants, with nitrogen content affecting its pyrolysis rate and thermal stability. This study creates all-atom models of NC with varying nitrogen levels to explore pyrolysis mechanisms and validate them against experimental thermal response data. Results show that $RO-NO_2$ bond cleavage initiates NC decomposition. Lower nitration levels convert nitrogen oxides into carbon-nitrogen compounds, primarily HCN. Additionally, HCHO production is linked to CH_2ONO_2 group transformation, with low-nitration, high-hydrogen NC reducing HCHO yield. Kinetic parameters for cellulose thermal decomposition indicate that pyrolysis activation energies decrease with nitration levels, demonstrating that nitration significantly lowers the energy barrier for ring-opening. Molecular dynamics simulations reveal pathways for HCHO, NO_2, and NO generation during combustion, enhancing understanding of NC combustion mechanisms and safety in explosive applications.

KEYWORDS
kinetic, nitrocellulose, nitrogen content, pyrolysis mechanism, ReaxFF molecular dynamics

1 | INTRODUCTION

Nitrocellulose (NC) is a significant class of semirigid chain natural polymer derivatives, comprising a mixture of cellulose nitrates.[1,2] It is widely used in the production of energetic materials such as monopropellants, bipropellants, tripropellants, and explosives.[3] Its utility spans across military, chemical, and aerospace industries due to its high flammability and energy density. However, its inherent instability and self-catalytic nature introduce critical safety concerns, particularly in its storage and transportation, which are strongly influenced by its nitrogen content. High-nitration NC (>12%) is commonly used in gunpowder and propellants, while low-nitration NC (<12%) finds applications in colloid production.[4,5] The relationship between nitrogen content and thermal stability has been established, with higher nitrogen content correlating with lower thermal stability.[6]

Previous studies on the pyrolysis of NC have predominantly focused on the influence of additives on its thermal stability. Techniques such as thermogravimetric analysis have been employed to measure the decomposition rate and thermal stability of

Changwei Liu and Haojie Qian Contributed equally to this work.

NC, evaluating its pyrolysis characteristics and thermodynamic parameters. Chai et al.,[3] after qualitatively and quantitatively analyzing the macroscopic and microscopic structures of NC samples with varying nitrogen content, observed a correlation between higher nitrogen content and an increase in the number of nitro groups and cracks on the fiber surface. They found that the pyrolysis of NC primarily occurs within the temperature range of 180–240°C, with the initial nitrogen oxides produced being nitrogen dioxide (NO_2). Similarly, Shao et al.[7] proposed a thermal decomposition mechanism for NC and provided a generalized classification of the entire process. Furthermore, based on experimental characterization, Rychly et al.[8–10] speculated on the positions of significant chemical bond ruptures. However, due to the inherent risks associated with energetic materials during experimental procedures, a comprehensive understanding of the influence of nitrogen content and temperature on the pyrolysis behavior of NC and its molecular mechanisms is still lacking. Traditional experimental methods face challenges in dealing with the high dimensionality and heterogeneity of material data, leading to limited generalization capabilities and insufficient information representation.[11,12] For energetic materials, studying how the introduction of nitro substituents affects their thermal decomposition mechanisms at the molecular level is advantageous for enhancing our understanding of their energy release mechanisms and safety considerations. Therefore, understanding the following processes is crucial: (i) the reaction mechanisms of cellulose during the initial stages of pyrolysis and combustion; (ii) the comparative analysis of bond dissociation and ring-opening kinetics during pyrolysis; and (iii) how nitration and esterification reactions on cellulose promote its dissociation process. However, both experimentally and theoretically, research on such topics is still in its infancy, and explanations for the above three questions remain elusive.

Additionally, the inherent risks associated with handling energetic materials experimentally restrict the scope of traditional experimental approaches, which often fail to capture the complex, high-dimensional dynamics of material decomposition. Recent advances in molecular dynamics simulations, particularly using the ReaxFF reactive force field, provide a promising avenue to overcome these challenges.[13–15] The ReaxFF has been successfully applied in numerous studies, providing profound insights into the reactivity of materials, such as the high-temperature pyrolysis of CL20 – TNT eutectics,[16–18] the temperature effects on hydrazine decomposition,[19,20] and the thermal decomposition mechanisms of trinitrophenol.[21,22] By simulating the molecular mechanisms underlying NC pyrolysis, it is possible to gain unprecedented insights into bond dissociation, nitrogen oxide formation, and the overall thermal decomposition process, offering a pathway to enhance the safety and efficiency of NC-based materials.

Given these gaps in current research, this study aims to explore the molecular-level mechanisms of NC pyrolysis with a focus on the effects of nitrogen content. By employing ReaxFF molecular dynamics simulations, this research seeks to uncover the kinetics of bond dissociation, the formation of key small molecules such as NO_2, NO, and HCHO, and the influence of nitrogen content on the overall pyrolysis activation energy. These findings are expected to contribute to the safer handling of NC and improve its application in high-energy systems.

2 | MODEL AND METHODS

2.1 | Model description

The high crystallinity of natural cellulose renders it insoluble in water, with most chemical reactions occurring in multiphase systems. The crystalline regions of cellulose impede the entry of reactants, affecting the uniform progress of modification reactions and exhibiting characteristics of layer-by-layer reactions and nonuniformity. Therefore, to investigate the influence of nitration reactions on the pyrolysis mechanism of cellulose, hydroxyl hydrogen on the furan ring is subjected to varying degrees of nitro substitution, including single, double, and triple nitro substitutions, as shown in Figure 1B–D. Due to the structural features of cellulose molecules and the heterogeneous and layer-by-layer nature of nitration reactions, the nitrogen content distribution of NC exhibits nonuniformity. Thus, a normal probability distribution is adopted to randomly mix the three different nitro-substituted NC monomers, constructing three NC long chains with different nitrogen contents and nonuniform distributions, as shown in Table 1. The nitrogen contents are 11.63% (low nitration), 11.97% (boundary nitration), and 12.60% (high nitration), respectively, where a nitrogen content of 12 wt% is typically considered the boundary between highly and lowly nitrated cellulose.[3,23]

2.2 | Simulation method and parameter configuration

For the unmodified cellulose system, we employed the force field parameters for carbon combustion developed by Castro-Marcano,[24] which have been demonstrated to apply to fuel pyrolysis and gasification processes involving C/H/O compounds.[25,26] For the cellulose system modified with nitroesters, we utilized a C/H/O/N/S force field.[19] This force field offers significant advantages in describing N – O and N – C bonds and has been successfully applied in numerous studies of high-energy materials, including the high-temperature pyrolysis of CL20 – TNT eutectics,[16–18] temperature effects on hydrazine decomposition,[19,20] and thermal decomposition mechanisms of trinitrophenol.[21,22] The core of the ReaxFF reactive force field is the bond order (BO_{ij}), which defines interatomic interactions. It categorizes the contributions of individual interactions into bond, angle, dihedral, conjugation, Coulombic, van der Waals, and adjustment terms, which are illustrated below:

$$E_{system} = E_{bond} + E_{lp} + E_{over} + E_{under} + E_{val} + E_{pen} + E_{coa} + E_{C2} + E_{triple} + E_{tors} + E_{conj} + E_{H-bond} + E_{vdWaals} + E_{Coulomb} \quad (1)$$

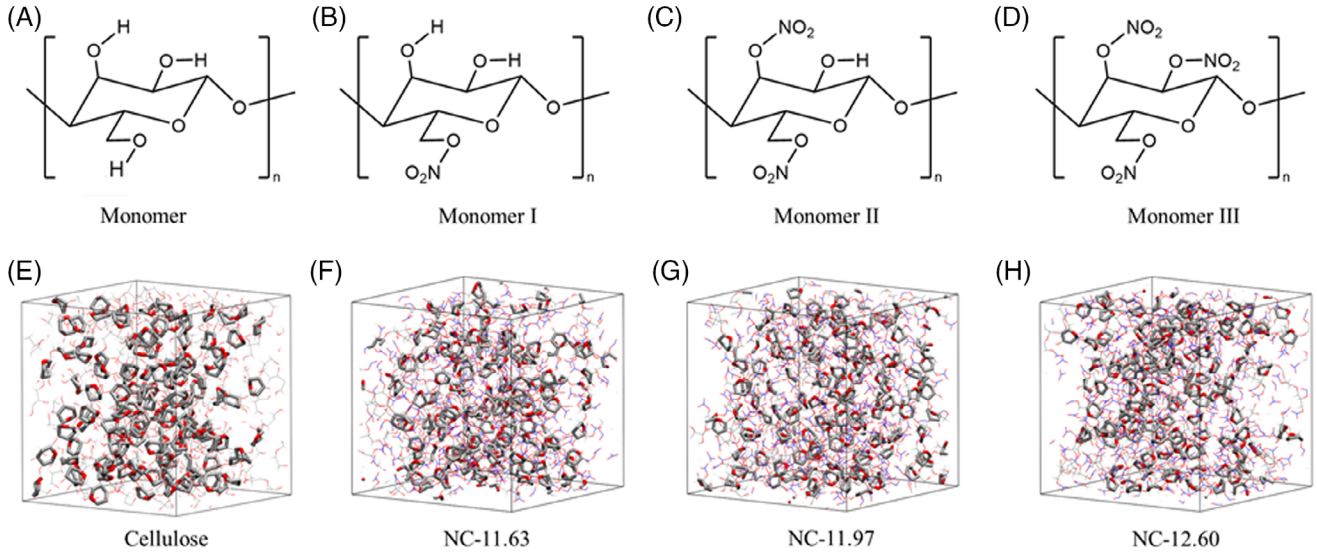

FIGURE 1 Cellulose monomers and conformations of NC monomers with different degrees of nitro substitution: (A) unsubstituted monomers, (B) mononitro-substituted monomers I, (C) dinitro-substituted monomers II, (D) trinitro-substituted monomers III. Construction of cellulose condensed-phase systems: (d) Cellulose, (E) NC − 11.63, (F) NC − 11.97, (G) NC − 12.60 system. The pyran ring structure takes the Licorice display format.

TABLE 1 Parameters of three nitrogen content (NC) model systems.

Models	Nitrogen[a] content	Cellulose (wt%)	Monomer I (wt%)	Monomer II (wt%)	Monomer III (wt%)	Degree of polymerization	Density/g·cm^{-3}
Cellulose	0	100	0	0	0	80	1.2
NC − 11.63	11.63	0	28.8	27.5	43.8	80	1.2
NC − 11.97	11.97	0	25	25	50	80	1.2
NC − 12.60	12.60	0	17.5	20	62.5	80	1.2

[a]Nitrogen content is as mass fraction.

Among these, E_{bond}, E_{val}, and E_{tors} represent bond-level pairwise interaction potentials, while $E_{vdWaals}$ denotes intermolecular interaction potential, $E_{Coulomb}$ represents electrostatic interaction potential, and $E_{H\text{-}bond}$ signifies hydrogen bond interaction potential. The bond-level BO_{ij} is defined as a function of interatomic distance, with the functional relationship as follows:

$$BO'_{ij} = BO^{\sigma}_{ij} + BO^{\pi}_{ij} + BO^{\pi\pi}_{ij} = \begin{aligned} &exp\left[p_{bo1}\cdot\left(\frac{r_{ij}}{r^{\sigma}_{o}}\right)^{p_{bo2}}\right] \\ &+exp\left[p_{bo3}\cdot\left(\frac{r_{ij}}{r^{\pi}_{o}}\right)^{p_{bo4}}\right] \\ &+exp\left[p_{bo5}\cdot\left(\frac{r_{ij}}{r^{\pi\pi}_{o}}\right)^{p_{bo6}}\right] \end{aligned} \quad (2)$$

BO^{σ}_{ij}, BO^{π}_{ij}, and $BO^{\pi\pi}_{ij}$ respectively denote the uncorrected bond orders for σ, π, and π-π bonds, while r_{ij} represents the distance between atoms, with corresponding equilibrium distances r^{σ}_{0}, r^{π}_{0}, and $r^{\pi\pi}_{0}$. $P_{bo1} \sim P_{bo6}$ represent empirical regression parameters. All simulations are conducted with periodic boundary conditions in the *x*, *y*, and *z* directions. Initial structural energy minimization is carried out to achieve the configuration of the system at the local potential energy minimum. To ensure the rationality of the initial structure, dynamic structural relaxation is performed in the NPT ensemble (constant number of atoms, pressure, and temperature), with the initial temperature held at 298.15 K, utilizing the Nose-Hoover thermostat[27] with a time step of 0.1 fs for 2×10^5 steps (approximately 20 ps) of simulation. Subsequently, cook-off simulations are conducted in the NVT ensemble (constant number of atoms, volume, and temperature), where cellulose and its modified systems are rapidly heated from 298.15 K to the specified temperatures (1500 K, 2000 K, and 3000 K) at a rate of 400 K/ps, employing the Berendsen thermostat with a damping coefficient of 100 fs and a time step of 0.1 fs for 2×10^6 steps (approximately 200 ps) of simulation at the designated temperature. A smaller time step ensures the stability of the pyrolysis process and the reliability of bond order sampling. Independent dynamic sampling is conducted for each of the three systems. Additionally, to investigate the pyrolysis mechanism of systems with different nitrogen contents, single-cycle slow heating annealing simulations are performed. The system temperature is raised from 300 to 2300 K at a rate of 7.5 K/ps and then rapidly annealed back to 300 K, maintaining consistency with all other parameter configurations and isothermal pyrolysis processes. A cutoff distance of 0.3 bond orders is employed to identify extracted molecular

fragments and bond order changes. All MD simulations are carried out using the Large-scale Atomic/Molecular Massively Parallel Simulator (LAMMPS),[28,29] with bond order and atomic trajectories saved every 500 steps for subsequent bond analysis and species distribution analysis, employing a protocol $BO_{ij} = 0.3 \sim 1.3$, $1.3 \sim 2.3$ to statistically analyze single and double bond evolution mechanisms.

3 | RESULTS AND DISCUSSION

3.1 | Effects of temperature and nitrogen content

For the pyrolysis of cellulose, up to 4050 reaction intermediates were observed at 3000 K, of which formic acid and multiple alcohol derivatives were the main species formed, as shown in Figures S1 and S2. However, nitrate esterification has a great influence on the pyrolysis products of cellulose. For low nitrification, border nitration, and highly NC pyrolysis, abundant experimental studies have demonstrated that small molecular species such as NO_2, NO, HCHO, H_2O, CO_2, and CO are crucial products generated during the pyrolysis of NC. Simulation snapshots indicate (Figure 2) that during the initial stages of simulation, dissociation of the O – NO_2 bond takes precedence, yielding NO_2 species. This is attributed to the relatively low dissociation energy of the O – NO_2 bond, making its rupture a pivotal factor triggering the decomposition of NC. As depicted in Figure 3A, the onset temperature for NO_2 generation is around 700 K. With increasing temperature, the NO_2 content initially exhibits a linear increase, followed by a linear decrease, reaching its peak around

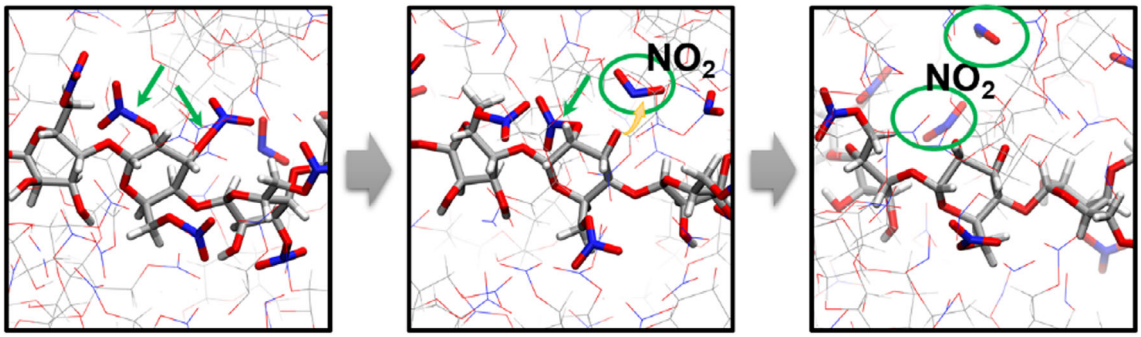

FIGURE 2 Snapshot of the initial simulation generated by NO_2.

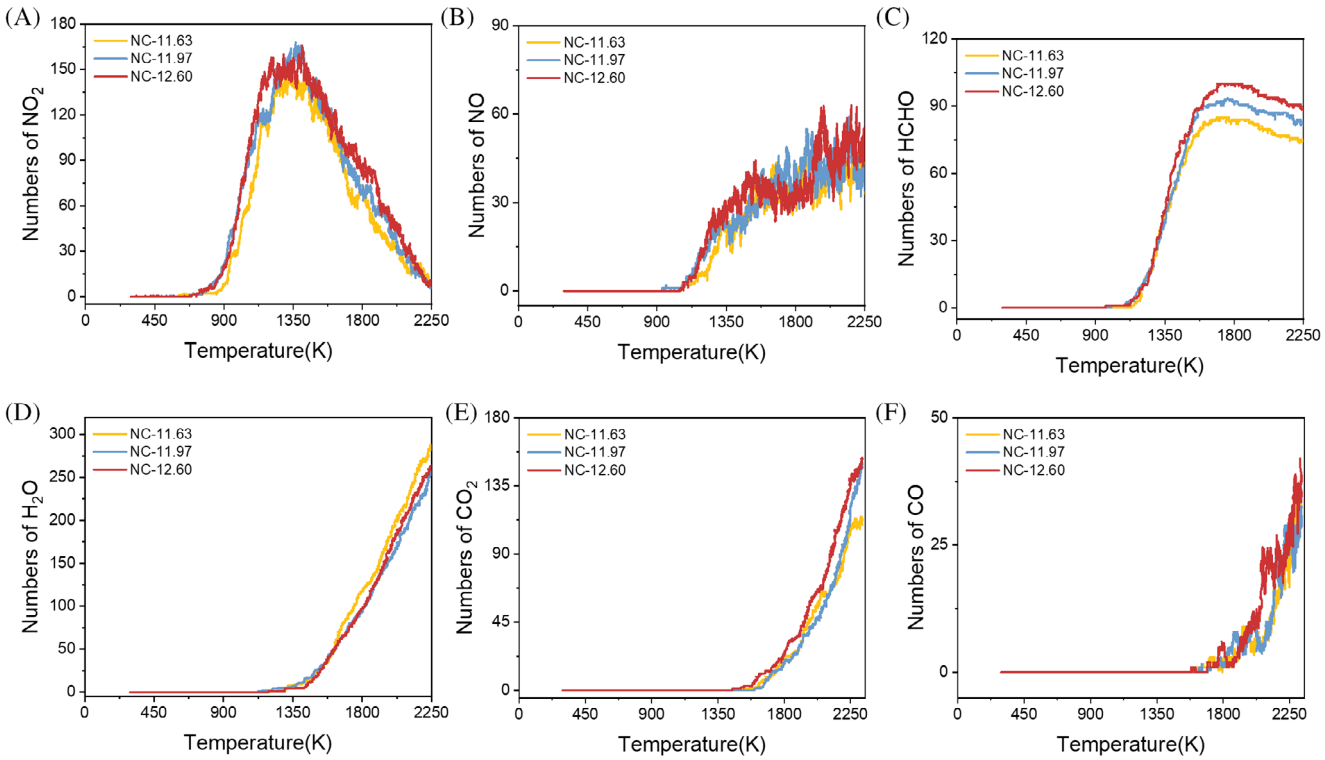

FIGURE 3 Statistical distribution of major light gases after nitrocellulose pyrolysis under different nitrogen content at the heating stage. (A) NO_2 species, (B) NO species, (C) HCHO species, (D) H_2O species, (E) CO_2 species, and (F) CO species.

1350 K, indicating nearly complete denitration of NC at this temperature. Furthermore, for low-nitration NC systems (NC − 11.63), the initial generation temperature of NO_2 shifts to the right, and it can be observed that the higher the nitrogen content, the lower the temperature at which NO_2 peaks. The initial response temperature of NO species is around 1000 K (Figure 3B), indicating that during the early stages of pyrolysis, the primary nitrogen oxide produced is NO_2 species. This is because NO_2 species undergo rearrangement during pyrolysis to form nitrite (*ONO), which upon bond cleavage forms NO. Formaldehyde molecules are generated at around 1100 K, with nitrogen content significantly influencing HCHO content; the higher the nitrogen content, the more HCHO molecules are produced (Figure 3C). For other inorganic small molecules such as H_2O, CO_2, and CO species, as shown in Figure 3D–H, the initial response temperatures are approximately 1250, 1500, and 1550 K, respectively, unaffected by nitrogen content. Notably, low-nitration NC systems can produce more water molecules due to the presence of more hydroxyl functional groups in these systems. The generation of CO_2 and CO indicates dissociation decarbonylation of the pyran ring, while NC systems above the boundary nitration level seem to favor deeper decarbonylation of the carbon chain.

In NC, the C − C, C − O, C − N, and N − O bonds are the predominant chemical bonds, playing crucial roles in the dissociation kinetics of NC, and are of significant importance for validating the consistency between experimental results and simulation values.[30] Figure 4 illustrates the evolution patterns of important chemical bonds in three different NC systems at various temperatures. During the initial rapid heating stage, some bonds inevitably rupture, but the crucial aspect lies in the trends during the subsequent 200 ps isothermal process. During the constant-temperature stage at 3000 K, the quantity of C − C bonds initially decreases and then increases (Figure 4I), while at moderate to low temperatures (1500 K and 2000 K), it consistently decreases (Figure 4A,E), indicating carbonization induced by high-temperature pyrolysis. Additionally, in highly nitrated NC systems, there is a greater extent of C −C bond dissociation, possibly due to the easier dissociation of C − C bonds between adjacent acyl groups formed after NO_2 removal.[3] The quantity of C − O bonds initially decreases rapidly and then increases, with highly nitrated NC systems exhibiting a higher number of generated C − O bonds compared with low-nitration systems, attributed to the higher oxygen content in highly nitrated NC and moderate temperatures (2000 K) favoring deeper carbon oxidation. Furthermore, at moderate to high temperatures, the produced NO_2 and HCHO species undergo autocatalytic reactions between the pyran glucose ring framework, forming a significant amount of C − N bonds, suggesting the potential generation of hydrogen cyanide (HCN) species.[31] We observe that low-nitration NC systems seem to more readily produce HCN gas, while the rate of decline of N − O

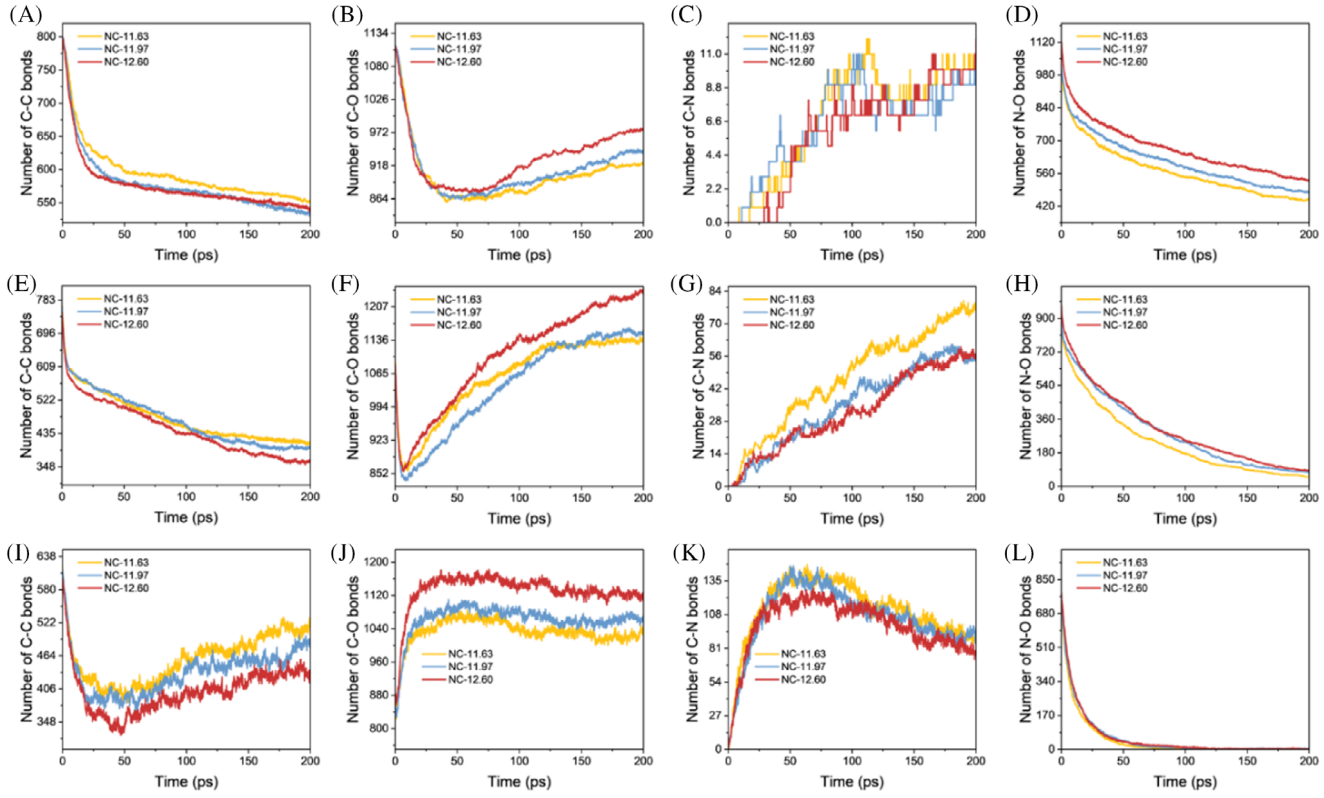

FIGURE 4 Evolutionary behavior of C − C bonds, C − O bonds, C − N bonds, and N − O bonds in nitrocellulose systems with three nitrogen contents derived from simulations with simulation time in the 1500–3000 K range. (A) ∼ (D): 1500 K; (E) ∼ (H): 2000 K; (I) ∼ (L): 3000 K.

bonds in low-nitration NC systems is higher than in highly nitrated systems (Figure 4D,H), further indicating the transformation from nitrogen oxides to carbon-nitrogen compounds.

Figure 5 illustrates the distribution of pyrolysis gases over time in NC systems with different nitrogen contents at a temperature of 3000 K. During the later stages of pyrolysis, light gas products mainly consist of small molecular species such as H_2O, N_2, CO_2, and CO, with their quantities remaining relatively stable over the simulation period, indicating that the pyrolysis reaction has reached a thermal equilibrium state. In the initial stages of pyrolysis experiments at 3000 K, NO_2 species appear first, and with increasing nitrogen content, the response peak of NO_2 species becomes higher. As the concentration of NO_2 species begins to decline, species such as HCHO, NO, H_2O, CO_2, CO, and N_2 appear successively, consistent with the temperature response during the heating process. Moreover, formaldehyde molecules increase with increasing nitrogen content. As shown in Figure 6, formaldehyde is derived from the decomposition of the RCH_2ONO_2 group. NO_2, generated initially from this decomposition, acts on the condensed phase, triggering autocatalytic reactions that promote the rupture of C – C bonds and oxygen bridge bonds between adjacent carbonyl groups, subsequently releasing HCHO gas. However, during the pyrolysis process, the produced amine substances undergo condensation reactions with formaldehyde, and formaldehyde also decomposes under high-temperature conditions to

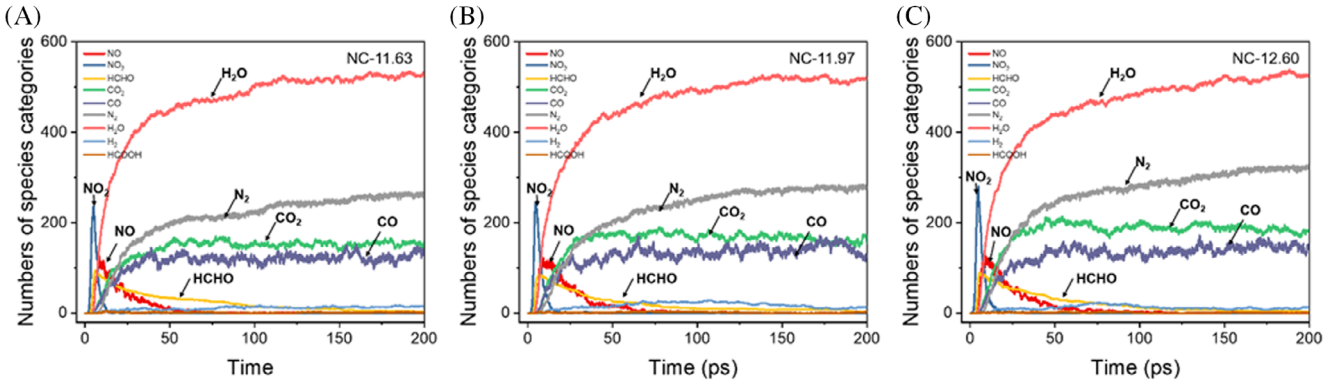

FIGURE 5 The distribution of main light gas products in the whole process of nitrocellulose pyrolysis with different nitrogen content at 3000 K. (A) Nitrogen content of 11.63%; (B) nitrogen content of 11.97%; (C) nitrogen content of 12.60%.

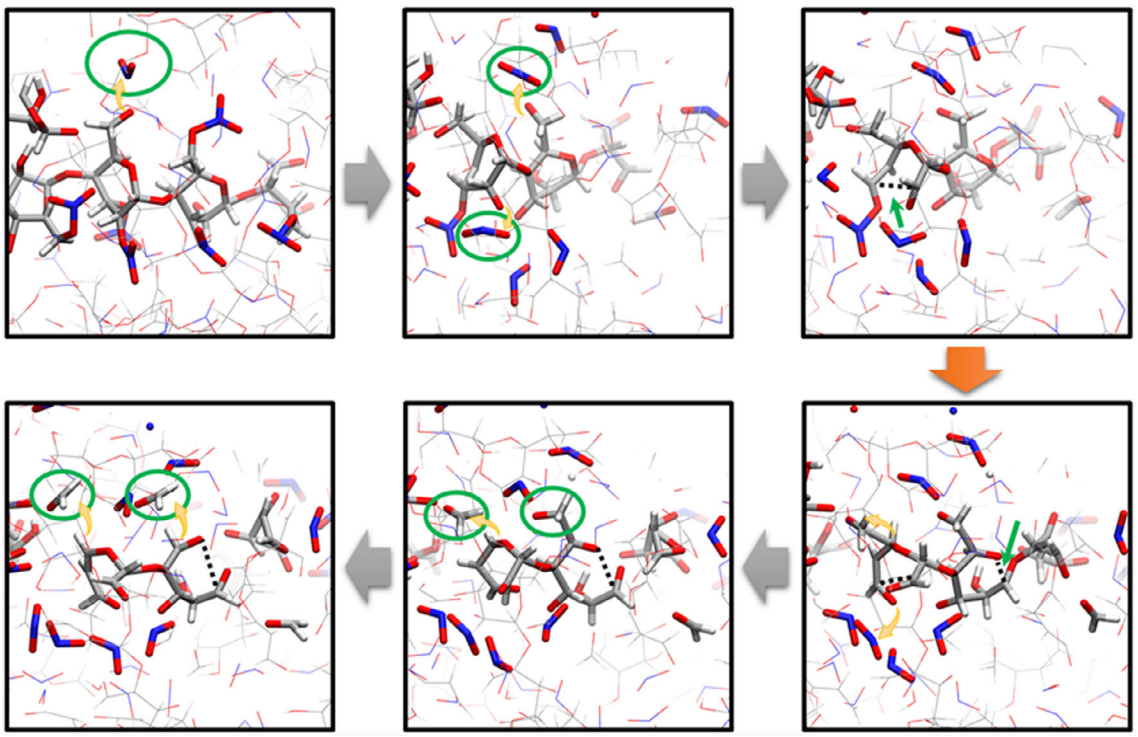

FIGURE 6 Snapshots of NC pyran ring-opening simulations.

produce water and carbon dioxide, ultimately leading to a decrease in HCHO content. Additionally, we observe trace amounts of hydrogen gas generated during the pyrolysis process, possibly originating from the high-temperature decomposition of hydrocarbon intermediates. The formation of HCOOH species typically begins after most species have appeared. Brill et al.[23] proposed that HCOOH is a species formed from further decomposition of condensed-phase products. The observed relatively low content of formic acid and hydrogen gas is within the time scale of our simulations. Finally, among the four stable products (H_2O, CO, CO_2, and N_2), except for the content of water molecules, which remains almost unchanged with changes in nitrogen content, the quantities of CO, CO_2, and N_2 products increase with increasing nitrogen content, indicating that higher nitrogen content contributes to more thorough pyrolysis.

3.2 | Kinetic rate analysis of pyrolysis

The evolution trends of potential energy at different temperatures in low-nitration, boundary-nitration, and high-nitration NC systems are crucial for understanding the influence of nitrogen content on pyrolysis. As depicted in Figure 7A–C, with increasing pyrolysis temperature, the potential energy curves converge more rapidly. Within the first 0 to 50 ps, at a temperature of 3000 K, the potential energy curve declines more rapidly, then begins to approach a dynamic equilibrium state, while at 2000 K, the potential energy curve decreases more slowly, indicating that higher temperatures lead to faster system equilibrium, which is reasonable for describing combustion processes. The degree of decline in potential energy curves in the three temperature ranges changes with increasing nitrogen content, with higher nitrogen content resulting in a faster decline in system potential energy within the same time frame. The rate of decline in system potential energy is closely related to the exothermic reaction process and strongly depends on temperature. This process can be described by an exponential function relationship:

$$U(t) = U_0 + \Delta U \cdot \exp\left[\frac{-(t - t_{E-I})}{\tau}\right] \quad (3)$$

U_0 represents the asymptotic potential energy when the products tend to equilibrium, ΔU is the heat released by the reaction, $t_{E\text{-}I}$ is the equilibrium and induction time before the decomposition reaction occurs, and τ is the overall characteristic time of the reaction. The thermal decomposition of NC at high temperatures follows the Arrhenius law, where the influence of temperature on the pyrolysis reaction can be expressed as

$$k(T) = \frac{1}{\tau} = A \cdot \exp\left(-\frac{E_a}{RT}\right) \quad (4)$$

Consequently:

$$\ln\{k\} = -\ln\tau = -\frac{E_a}{RT} + \ln A \quad (5)$$

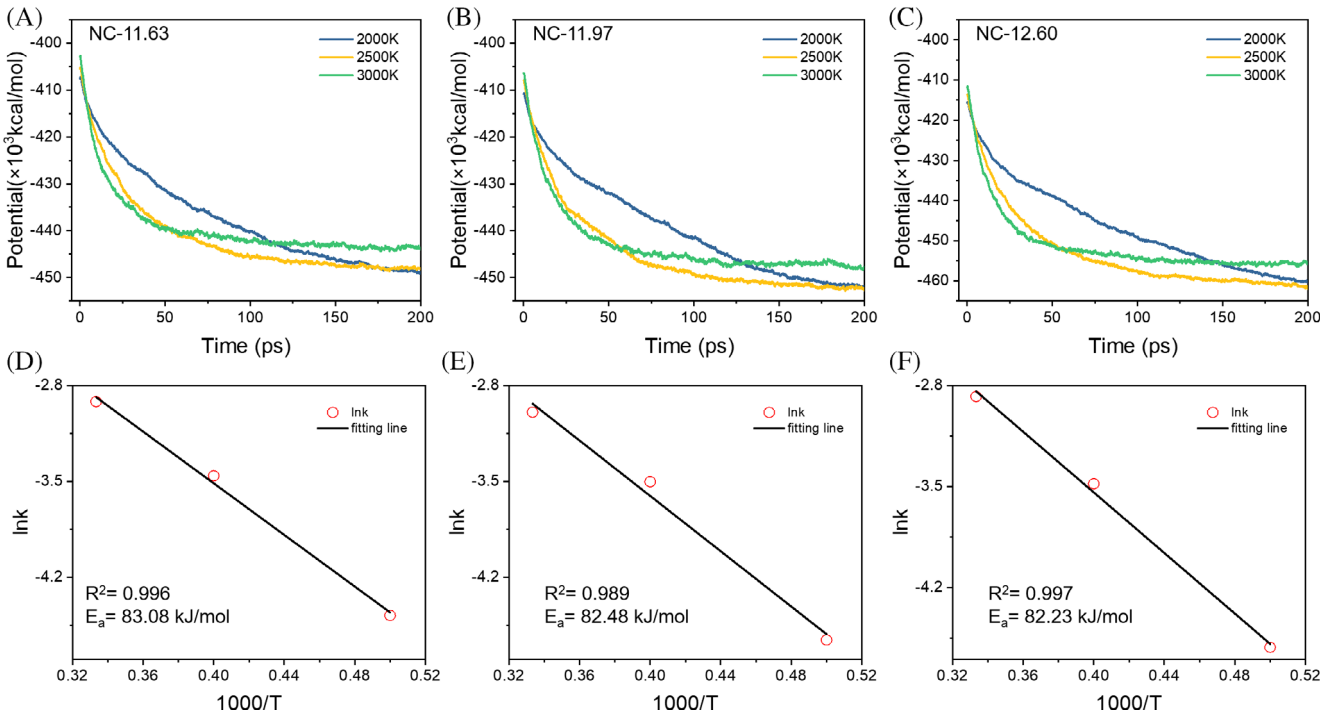

FIGURE 7 Isothermal potential energy curves of nitrocellulose under different nitrogen contents and temperature-dependent dissociation rates (*k*) of potential energy during the pyrolysis process. (A) and (D) are statistics based on the NC- 11.63 system; (B) and (E) are statistics based on the NC − 11.97 system; (C) and (F) are statistics based on the NC- − 12.60 system.

From this, we can obtain the rate constants {k} at various temperatures and acquire the activation energies of the pyrolysis process. The activation energies for the NC − 11.63, NC − 11.98, and NC − 12.60 systems are respectively 83.08 kJ/mol, 82.48 kJ/mol, and 82.23 kJ/mol. These values are comparable with those obtained by Duan et al.[32] based on the CALVET heat flow calorimeter C80 experiment for different nitrogen contents, NC. As the nitrogen content increases, there is a slight decrease in the activation energy of NC pyrolysis. Consequently, the stability of NC decreases with increasing nitrogen content, and higher nitrogen content often leads to easier decomposition of NC.[4,23]

The kinetic rate calibration of the N-O bond in NC was performed at temperatures of 1500, 2000, and 3000 K, with corresponding nitrogen contents of 11.63%, 11.97%, and 12.60%. For the dissociation kinetics analysis, the reaction rate constant is assumed to follow a power-law reaction, with the catalyst surface coverage maintained as a constant. According to the Arrhenius equation, the reaction rate is expressed as

$$-\frac{dc(\text{N-O})}{dt} = kc(\text{N-O})^{\theta} \tag{6}$$

$$\ln\frac{c_t}{c_0} = -kt \tag{7}$$

$$\ln k = \ln A - \frac{E_a}{RT} \tag{8}$$

In this equation, k represents the kinetic rate constant for bond dissociation; c_t denotes the concentration of the N − O bond at time t; c_0 indicates the initial concentration of the N − O bond; R is the molar gas constant ($R = 8.31466\ \text{J·mol}^{-1}\text{·k}^{-1}$); A is the frequency factor; T represents the temperature; E_a denotes the intrinsic activation energy at that temperature; and is the reaction order. As shown in Figure 8A–C, the logarithm of the N − O bond concentration exhibits a linear relationship with time, confirming that the N − O bond reaction follows first-order kinetics ($\theta = 1$). Subsequently, we developed the kinetic equations for the dissociation of the N − O bond in low-nitrification, borderline nitrification, and high-nitrification scenarios, as illustrated in Figure 8D. It was found that the dissociation energy barrier of the N − O bond in cellulose with low nitrification is the highest (74.60 kJ/mol), while the activation energies for dissociation in borderline nitrification and high-nitrification systems are 67.37 and 67.22 kJ/mol, respectively. Furthermore, the dissociation rate of the N − O bond is greatest in the low-nitrification system, further validating that the N − O bond in low nitrification is more prone to undergo further hydrogenation and dissociation processes.

We observe that the opening kinetics of the pyranose glucose ring also satisfy first-order reaction kinetics. As depicted in Figure 9A,C,

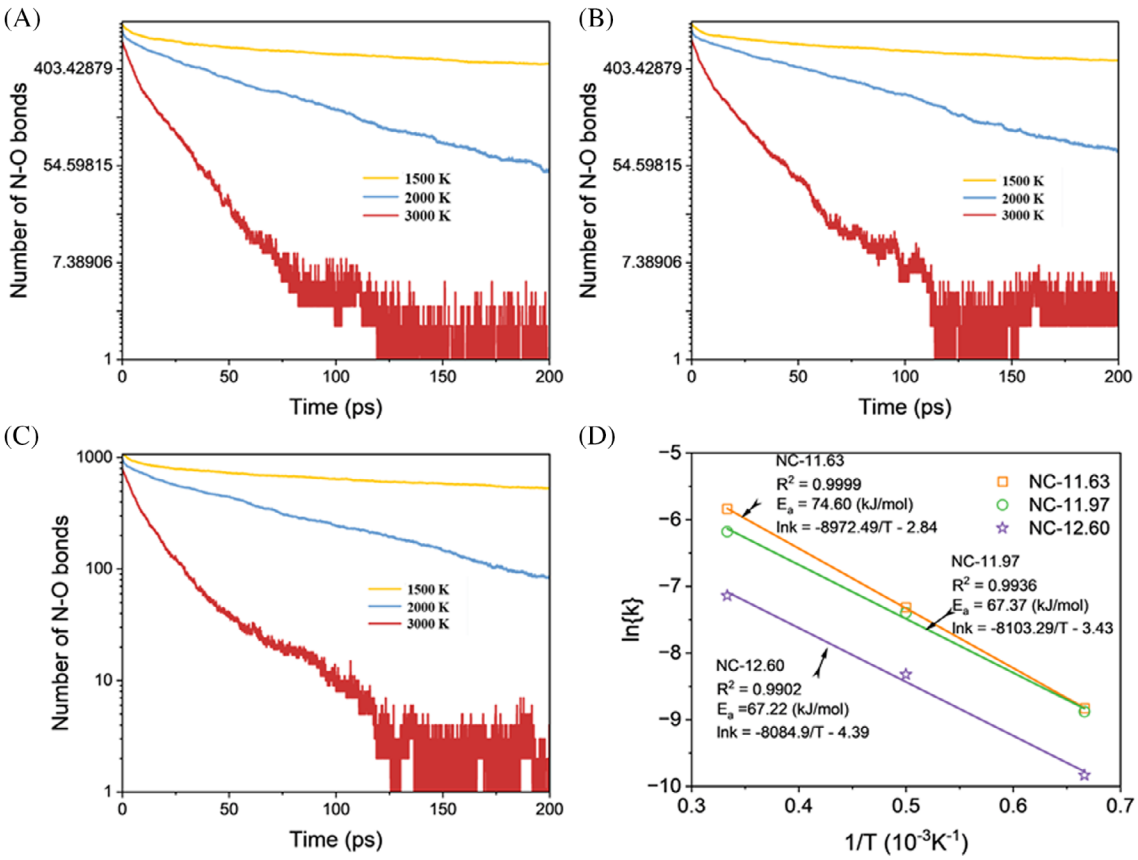

FIGURE 8 Isothermal N-O bond dissociation curves for the primary reaction kinetics of nitrocellulose at different nitrogen contents. (A) 11.63%, (B) 11.97%, and (C) 12.60%. (D) Temperature-dependent dissociation kinetic rates of N-O bonds.

during the initial stages of pyrolysis, the hexagonal ring structures rapidly dissociate, with a higher nitrogen content correlating to a faster rate of ring-opening. Furthermore, at temperatures reaching 3000 K, during the later stages of pyrolysis between 50 and 200 ps, the abundance of hexagonal rings begins to increase, particularly in systems with lower nitration. This indicates the occurrence of partial carbonization in the deep pyrolysis stage, indicating the formation of oligomers and cyclization, which implies the system begins to carbonize and form graphene-like structures. Initially, at high temperatures, a significant amount of tricyclic ring structures can rapidly form, reaching a dynamic equilibrium around 25 ps (Figure 9B). The dissociation of C – O bonds, C – H bonds, and C – C bonds (pyranose ring cleavage) leads to the formation of active carbon atoms, which may result in the rearrangement of the carbon framework, giving rise to tricyclic ring structures. Tricyclic carbon ring structures serve as precursors for NC carbonization, and although higher nitration can promote the formation of tricyclic carbon rings (Figure 9B), systems with higher nitration exhibit lower levels of carbonization, indicating that the significant production of gases such as NO_2, NO, CO, and HCHO in highly nitrated systems inhibits further carbonization. Figure 9D illustrates the activation energy E_a for the pyranose ring dissociation in NC pyrolysis systems with low nitration, boundary nitration, and high nitration. For systems with nitration levels above the boundary-nitration degree, the nitrogen content has minimal effect on the activation energy for hexagonal ring cleavage ($E_{a(NC-11.97)} = 61.59$ kJ/mol, $E_{a(NC-12.60)} = 60.54$ kJ/mol), whereas for low nitration systems, the activation energy is significantly influenced, with $E_{a\ (NC-11.63)}$ approximately 69.94 kJ/mol. This indicates that NC systems exceeding the boundary-nitration degree are more prone to pyranose ring dissociation. Consequently, there exists an inverse relationship between nitrogen content and the thermal stability of NC; higher nitrogen content corresponds to the poorer thermal stability of NC, making ring-opening reactions more likely to occur.

3.3 | Pyrolysis and formation mechanism

Although previous studies have delved deeply into the light gas evolution from NC decomposition,[3,23] to our knowledge, this study marks the first observation at the molecular scale of the bond cleavage behavior during the degradation of NC with varying nitrogen content.

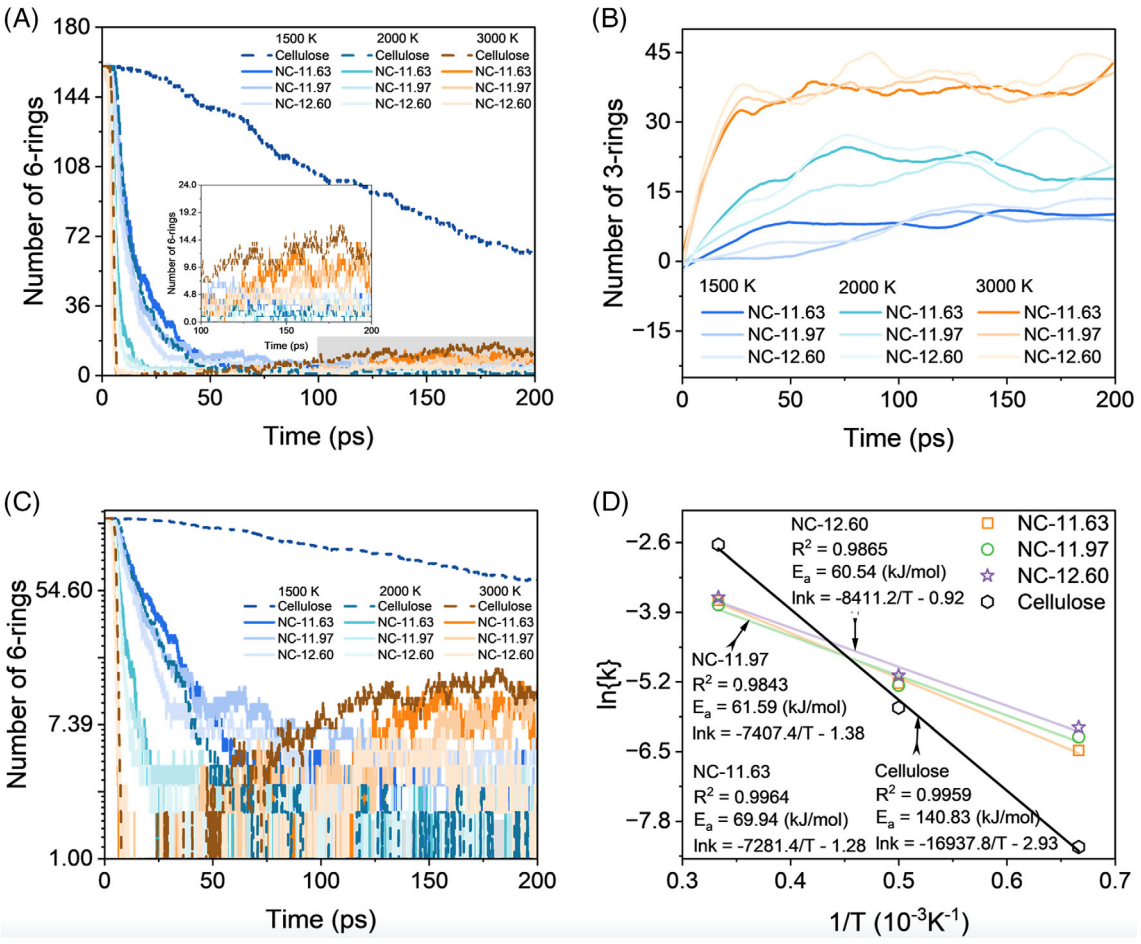

FIGURE 9 (A) Variation of the number of six-membered rings ($C_{6\text{-rings}}$) with time at different temperatures and nitrogen contents, (B) variation of three-membered rings ($C_{3\text{-rings}}$) with time. (C) Isothermal open-ring curves for the primary reaction kinetics of NC at different nitrogen contents. (D) Temperature-dependent dissociation rates {*k*} of $C_{6\text{-rings}}$ during the pyrolysis processes of NC.

The dissociation of the RO − NO_2 bond serves as the origin of pyrolysis. As depicted in Figure 10A, the disintegration of the trinitro-substituted pyranose ring initially results in the removal of two NO_2 groups, forming adjacent carbonyl groups. At this juncture, the C − C bond readily undergoes dissociation, yielding two R − CHO aldehyde groups. Subsequently, the oxygen bridge bonds within adjacent pyranose rings sequentially dissociate. The rupture of inter-ring ether bonds is pivotal in the transition of long-chain polymers to short-chain alkanes, as illustrated in Figure 10B. Following this, R − CHO dissociates to generate formaldehyde molecules, aligning with the previously discussed dissociation mechanism.

Although the three nitration levels of NC systems constructed contain identical amounts of RCH_2ONO_2 structures, the yield of formaldehyde (HCHO) is directly influenced by the evolution behavior of the CH_2ONO_2 group. The low-nitration NC system decreases the yield of HCHO species (Figure 3C). The study reveals four mechanisms for the evolution of the RCH_2O-NO_2 side chain group (Figure 11), namely: (a) direct denitration mechanism of the CH_2ONO_2

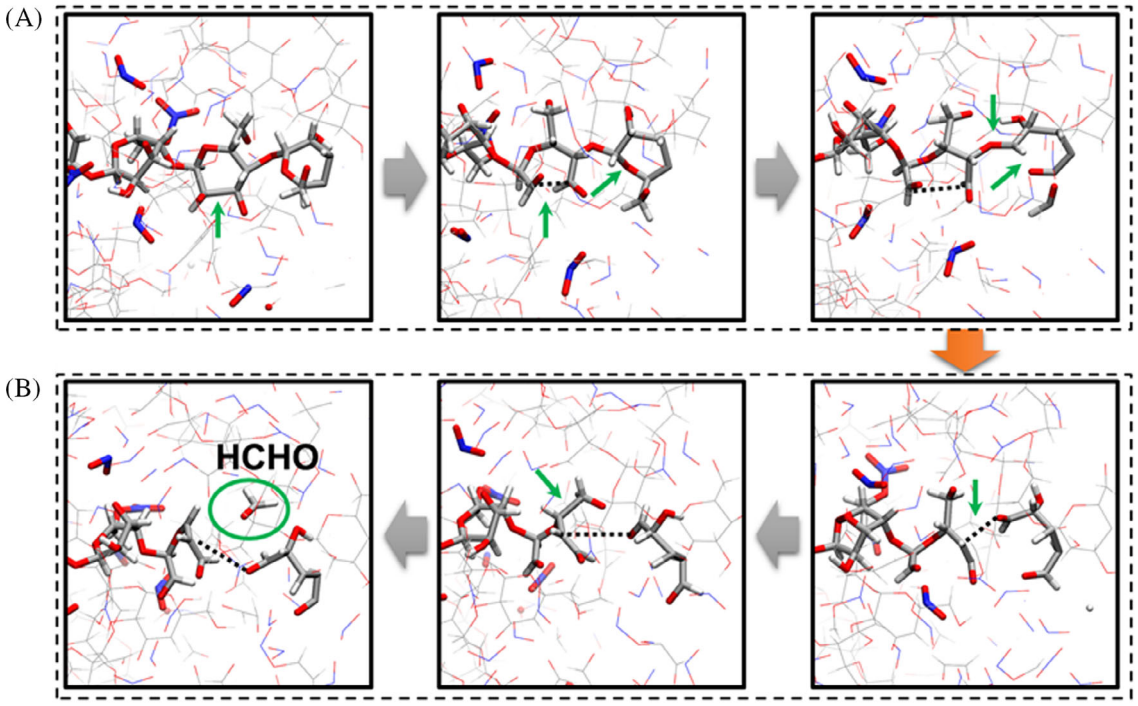

FIGURE 10 (A) Mechanism of carbonyl group formation, (B) Intercyclic ether bond dissociation and formaldehyde generation.

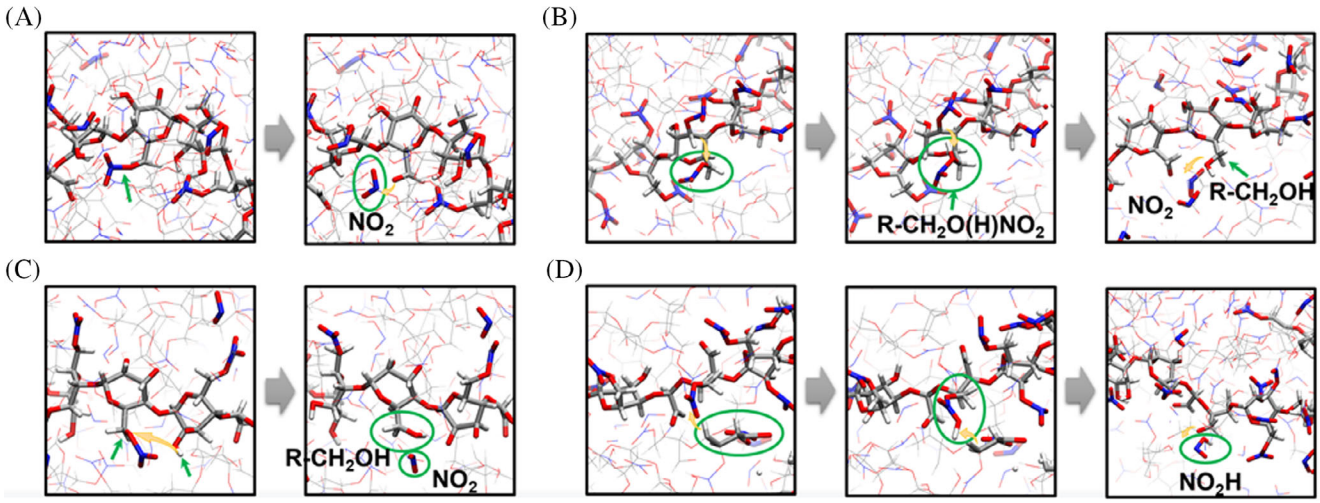

FIGURE 11 Snapshots of the evolution of the CH_2ONO_2 functional group in the pyranose ring Side Chain. (A) Direct NO_2 elimination process from CH_2ONO_2, (B) intra-ring hydrogenation of CH_2ONO_2 to NO_2 elimination process, (C) mechanism of hydrogenolysis of CH_2ONO_2 with the hydroxyl group of the neighboring ring to de-NO_2, and (D) hydroactivation of NO_2 in CH_2ONO_2 to generate NO_2H.

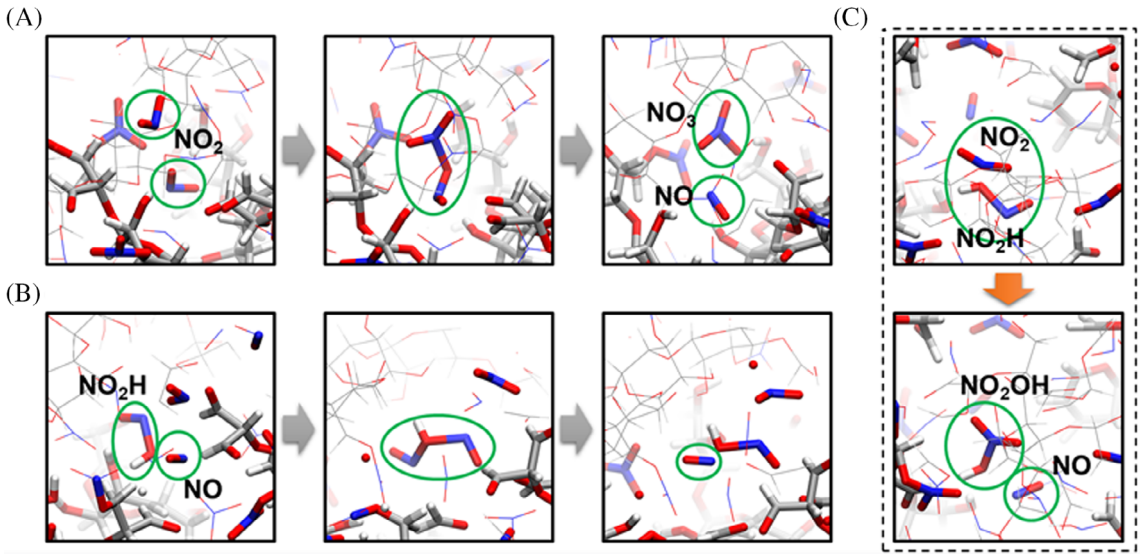

FIGURE 12 Three mechanisms for the generation of NO molecules. (A) NO bimolecular coupling mechanism for NO generation, (B) hydroxyl exchange reaction between NO_2H and NO, and (C) mechanism for NO_2H and reaction with NO_2 to generate NO molecules.

group, (b) intramolecular hydrogenation denitration mechanism of the CH_2ONO_2 group, (c) hydrogenolysis denitration mechanism of the CH_2ONO_2 group with adjacent ring hydroxyl groups, and (d) hydrogen activation denitration mechanism of NO_2 in the CH_2ONO_2 group to form NO_2H. The direct dissociation of the CH_2O-NO_2 bond is a crucial step in releasing the HCHO species (Figures 6 and 11A); however, due to the propensity of oxygen atoms in the CH_2ONO_2 group to undergo hydrogenation reactions, a portion of CH_2O-NO_2 bonds undergoes a process of hydrogenation before dissociation. In the intramolecular hydrogenation depicted in Figure 11B, the hydrogen atom on the pyranose ring, which is connected to the hydroxyl group substituted by NO_2, is easily activated, leading to the dissociation of the C-H bond and the formation of an O-H bond, resulting in the formation of the $CH_2O(H)NO_2$ group. Subsequently, the $CH_2O(H) - NO_2$ bond rapidly dissociates to form R-CH_2OH and NO_2 species. Similarly, when the unsubstituted OH group on the adjacent pyranose ring acts as a hydrogen donor, hydrogenation of the bridge oxygen atom in the CH_2ONO_2 group occurs, leading to the formation of R-CH_2OH, as depicted in Figure 11C. These processes collectively affect the subsequent generation of HCHO species. Due to the higher hydrogen content in low-nitration NC systems, the hydrogenation process of the R-CH_2OH group occurs more readily, resulting in a decrease in HCHO content. Furthermore, the NO_2 species can also undergo hydrogen activation, accompanying the pyrolysis reaction with the generation of nitrous acid (NO_2H),[10] as shown in Figure 11D. The formed NO_2H radical exhibits strong reactivity and further undergoes atomic exchange processes with NO_2 and NO in the gas phase. However, among all the mechanisms for the dissociation of R-CH_2ONO_2 moieties, mechanism (a) consistently occupies a predominant position in the dissociation of CH_2O-NO_2 bonds.

The NO species is a crucial product in the later stages of NC pyrolysis.[3] Based on reactive molecular dynamics simulation trajectories, we propose three mechanisms for the generation of NO molecules. Figure 12A illustrates the coupling process of two NO_2 species to produce NO and NO_3 species ($2NO_2 \rightarrow NO + NO_3$). In this process, the formation of NO is achieved through atomic rearrangement between NO_2 species. Additionally, we previously observed that the NO_2H species (Figure 11D) with an OH group readily captures NO and NO_2 molecules in the gas phase. Upon combination with NO, a nitrogen atom exchange reaction occurs, resulting in the formation of new NO and NO_2H radicals (Figure 12B). Conversely, upon combination with NO_2, one NO species and one NO_3H radical are released (Figure 12C). Therefore, the NO_2H radical plays a crucial mediating role in the generation of NO. In conclusion, NO species are generated through coupling exchange reactions between key nitrogen-containing compounds in the system, such as NO_2 and NO_2H. Understanding these mechanisms is essential for elucidating the impact of different nitrogen contents on the levels of key nitrogen-oxygen compounds.

4 | CONCLUSION

This study has provided a comprehensive and detailed molecular-level investigation into the pyrolysis mechanisms of NC with varying nitrogen content, utilizing advanced ReaxFF molecular dynamics simulations. By exploring the kinetics of bond dissociation, nitrogen oxide formation, and small molecule generation, we have revealed key insights into the thermal decomposition process of NC, which were previously not well understood at the molecular scale.

Key contributions of this work include:

1. Identification of bond dissociation pathways: We have confirmed that the cleavage of the $RO - NO_2$ bond is the primary trigger for NC decomposition, with nitrogen content playing a crucial role in

determining the onset of NO_2, NO, and HCHO production. These findings are essential for predicting and controlling the decomposition behavior of NC in high-energy systems.

2. Impact of nitrogen content on pyrolysis activation energy: Our study has demonstrated that higher nitrogen content significantly reduces the activation energy required for NC pyrolysis. This relationship highlights the trade-off between the energetic performance of NC and its thermal stability, offering critical insights for material design and safety management.
3. Novel molecular-level insights: Unlike previous studies that primarily relied on experimental approaches, our use of molecular dynamics simulations allowed for the investigation of the complex kinetics governing NC pyrolysis. The microscopic view of bond scission and reformation presented in this work fills a critical gap in the literature, offering unprecedented detail on the role of nitrogen content in NC decomposition.
4. Advancement in computational methods for energetic materials: This study showcases the power of ReaxFF molecular dynamics as a tool for analyzing the decomposition mechanisms of energetic materials like NC. The methodology applied here can be extended to other energetic materials, providing a safer and more detailed alternative to traditional experimental methods.

Implications of the findings: These findings contribute significantly to both the theoretical understanding and practical application of NC in high-energy systems. By uncovering the molecular pathways involved in NC pyrolysis, this study offers valuable information for optimizing NC formulations for safer storage, handling, and usage. Furthermore, the reduction in activation energy with increasing nitrogen content provides essential guidance for designing NC materials with improved performance and stability.

In conclusion, this work presents original and high-quality research that enhances the field's understanding of NC pyrolysis. The combination of advanced computational techniques and detailed molecular analysis sets a new benchmark for future studies on energetic materials, ensuring that the findings not only contribute to academic knowledge but also have practical applications in improving the safety and efficiency of high-energy systems.

AUTHOR CONTRIBUTIONS

Changwei Liu: Conceptualization; methodology; software; data curation; supervision; formal analysis; validation; investigation; visualization; writing – original draft; writing – review and editing. **Haojie Qian:** Conceptualization; methodology; software; validation; writing – original draft; supervision; investigation; visualization. **Qing Wang:** Writing – original draft. **Jinkai Qiu:** Visualization. **Yajun Ding:** Conceptualization; supervision; formal analysis; validation; investigation; funding acquisition; writing – review and editing; visualization; resources. **Cheng Lian:** Conceptualization; methodology; investigation; funding acquisition; writing – original draft; writing – review and editing; visualization; validation; formal analysis; project administration; data curation; supervision; resources. **Honglai Liu:** Conceptualization; funding acquisition; validation; project administration; resources; supervision; data curation; investigation.

ACKNOWLEDGMENTS

This work was sponsored by the National Key Research and Development Program of China (No. 2019YFC1906702), the Fundamental Research Funds for the Central Universities (No. 2022ZFJH004, and 2024SMECP05), the National Natural Science Foundation of China (No. 22475101), and Young Elite Scientists Sponsorship Program by CAST (No. 2022QNRC001).

CONFLICT OF INTEREST STATEMENT

The authors declare no competing financial interest.

DATA AVAILABILITY STATEMENT

The numerical data from Figures 3–5, 7–9 are available in the Numerical-data.zip file.

ORCID

Cheng Lian https://orcid.org/0000-0002-9016-832X

REFERENCES

1. Morris E, Pulham CR, Morrison CA. Structure and properties of nitrocellulose: approaching 200 years of research. *RSC Adv*. 2023;13(46):32321-32333.
2. Mattar H, Baz Z, Saleh A, et al. Nitrocellulose: structure, synthesis, characterization, and applications. *Wat Energy Food Environ J*. 2020;3:1-15.
3. Chai H, Duan Q, Cao H, Li M, Sun J. Effects of nitrogen content on pyrolysis behavior of nitrocellulose. *Fuel*. 2020;264:116853.
4. Pourmortazavi S, Hosseini S, Rahimi-Nasrabadi M, Hajimirsadeghi S, Momenian H. Effect of nitrate content on thermal decomposition of nitrocellulose. *J Hazard Mater*. 2009;162(2–3):1141-1144.
5. Saunders C, Taylor LJ. A review of the synthesis, chemistry and analysis of nitrocellulose. *J Energetic Mater*. 1990;8(3):149-203.
6. Jutier JJ, Harrison Y, Premont S, Prud'homme RE. A nonisothermal Fourier transform infrared degradation study of nitrocelluloses derived from wood and cotton. *J Appl Polym Sci*. 1987;33(4):1359-1375.
7. Shao Z, Wang WJ. *Structure and properties of cellulose nitrate*. National Defense Industry Press; 2011.
8. Rychlý J, Lattuati-Derieux A, Matisová-Rychlá L, Csomorová K, Janigová I, Lavédrine BJ. Calorimetry, degradation of aged nitrocellulose investigated by thermal analysis and chemiluminescence. *J Therm Anal Calorim*. 2012;107(3):1267-1276.
9. Berthumeyrie S, Collin S, Bussiere P-O, Therias S. Photooxidation of cellulose nitrate: new insights into degradation mechanisms. *J Hazard Mater*. 2014;272:137-147. doi:10.1016/j.jhazmat.2014.02.039
10. Neves A, Angelin EM, Roldão É, Melo MJ. New insights into the degradation mechanism of cellulose nitrate in cinematographic films by Raman microscopy. *J Raman Spectrosc*. 2019;50(2):202-212.
11. Wu X, Wang H, Gong Y, et al. Graph neural networks for molecular and materials representation. *J Mater Inform*. 2023;3(2):12.
12. Rao Y, Lu Y, Zhang L, et al. A metadata schema for lattice thermal conductivity from first-principles calculations. *J Mater Inform*. 2022;2(4):17.
13. van Duin ACT, Dasgupta S, Lorant F, Goddard WA. ReaxFF: a reactive force field for hydrocarbons. *Chem A Eur J*. 2001;105(41):9396-9409.
14. Nakano A. Parallel multilevel preconditioned conjugate-gradient approach to variable-charge molecular dynamics. *Comput Phys Commun*. 1997;104(1):59-69.
15. Senftle TP, Hong S, Islam MM, et al. The ReaxFF reactive force-field: development, applications and future directions. *Npj Comput Mater*. 2016;2(1):15011. doi:10.1038/npjcompumats.2015.11

16. Liu H, Li Q-K, He Y-H. Pyrolysis of CL20-TNT cocrystal from ReaxFF/lg reactive molecular dynamics simulations. *Acta Phys Sin*. 2013;62(20):208202.
17. Ren C, Liu H, Li X, Guo L. Decomposition mechanism scenarios of CL-20 co-crystals revealed by ReaxFF molecular dynamics: similarities and differences. *Phys Chem Chem Phys*. 2020;22(5):2827-2840.
18. Wang F, Chen L, Geng D, Wu J, Lu J, Wang C. Thermal decomposition mechanism of CL-20 at different temperatures by ReaxFF reactive molecular dynamics simulations. *J Phys Chem A*. 2018;122(16):3971-3979.
19. Zhang L, Duin ACT v, Zybin SV, Goddard WA Iii. Thermal decomposition of Hydrazines from reactive dynamics using the ReaxFF reactive force field. *J Phys Chem B*. 2009;113(31):10770-10778.
20. Jiang J, Zhao Y, Zhao F-Q, Xu S-Y, Ju X-H. The mechanism of methyl hydrazine degradation by supercritical water oxidation using ReaxFF simulation. *J Hazard Mater*. 2022;440:129832.
21. Zhang L, Zybin SV, van Duin ACT, Dasgupta S, Goddard WA, Kober EM. Carbon cluster formation during thermal decomposition of Octahydro-1,3,5,7-tetranitro-1,3,5,7-tetrazocine and 1,3,5-Triamino-2,4,6-trinitrobenzene high explosives from ReaxFF reactive molecular dynamics simulations. *J Phys Chem A*. 2009;113(40):10619-10640.
22. Xiang D, Xie X, Yao PJC. Atomistic insight into thermal decomposition of 1, 3, 5-Triamino-2, 4, 6-trinitrobenzene nanoparticles according to the ReaxFF molecular dynamics method. 2022;7(2):e202102465.
23. Chen JK, Brill TB. Thermal decomposition of energetic materials 50. Kinetics and mechanism of nitrate ester polymers at high heating rates by SMATCH/FTIR spectroscopy. *Combust Flame*. 1991;85(3):479-488.
24. Castro-Marcano F, Kamat AM, Russo Jr MF, van Duin AC, Mathews JPJC. Flame, combustion of an Illinois No. 6 coal char simulated using an atomistic char representation and the ReaxFF reactive force field. 2012;159(3):1272-1285.
25. Jin H, Wu Y, Guo L, Su X. Molecular dynamic investigation on hydrogen production by polycyclic aromatic hydrocarbon gasification in supercritical water. *Int J Hydrogen Energy*. 2016;41(6):3837-3843.
26. Castro-Marcano F, Russo MF, van Duin ACT, Mathews JP. Pyrolysis of a large-scale molecular model for Illinois no. 6 coal using the ReaxFF reactive force field. *J Anal Appl Pyrol*. 2014;109:79-89.
27. Bussi G, Donadio D, Parrinello M. Canonical sampling through velocity rescaling. *J Chem Phys*. 2007;126(1):014101.
28. Plimpton S. Fast parallel algorithms for short-range molecular dynamics. *J Comput Phys*. 1995;117(1):1-19.
29. Aktulga HM, Fogarty JC, Pandit SA, Grama AY. Parallel reactive molecular dynamics: numerical methods and algorithmic techniques. *Parallel Comput*. 2012;38(4):245-259.
30. Batuer A, Chen D, He X, Huang Z. Simulation methods of cotton pyrolysis based on ReaxFF and the influence of volatile removal ratio on volatile evolution and char formation. *Chem Eng J*. 2021;405:126633.
31. Shao Z, Wang W. *Structure and properties of nitrocellulose*. National Defence Industry and Technology; 2011:2-11.
32. Chai H, Duan Q, Jiang L, Gong L, Chen H, Sun JJC. Theoretical and experimental study on the effect of nitrogen content on the thermal characteristics of nitrocellulose under low heating rates. *Cellulose*. 2019;26:763-776.

SUPPORTING INFORMATION

Additional supporting information can be found online in the Supporting Information section at the end of this article.

How to cite this article: Liu C, Qian H, Wang Q, et al. Microscopic kinetics of scission and reformation in the pyrolysis of nitrocellulose. *AIChE J*. 2025;71(7):e18844. doi:10.1002/aic.18844